

Motor Protein Transport Along Inhomogeneous Microtubules

S. D. Ryan · Z. McCarthy · M. Potomkin*

the date of receipt and acceptance should be inserted later

Abstract Many cellular processes rely on the cell's ability to transport material to and from the nucleus. Networks consisting of many microtubules and actin filaments are key to this transport. Recently, the inhibition of intracellular transport has been implicated in neurodegenerative diseases such as Alzheimer's disease and Amyotrophic Lateral Sclerosis (ALS). Furthermore, microtubules may contain so-called *defective regions* where motor protein velocity is reduced due to accumulation of other motors and microtubule associated proteins. In this work, we propose a new mathematical model describing the motion of motor proteins on microtubules which incorporate a defective region. We take a mean-field approach derived from a first principle lattice model to study motor protein dynamics and density profiles. In particular, given a set of model parameters we obtain a closed-form expression for the equilibrium density profile along a given microtubule. We then verify the analytic results using mathematical analysis on the discrete model and Monte Carlo simulations. This work will contribute to the fundamental understanding of inhomogeneous microtubules providing insight into microscopic interactions that may result in the onset of neurodegenerative diseases. Our results for inhomogeneous microtubules are consistent with prior work studying the homogeneous case.

Keywords Mathematical Biology, Motor Proteins, Microtubules, Phase Transitions, Defective Transport

S. D. Ryan
Department of Mathematics and Statistics, Cleveland State University, Cleveland, OH 44115, USA
Center for Applied Data Analysis and Modeling, Cleveland State University, Cleveland, OH 44115, USA
E-mail: s.d.ryan@csuohio.edu

Z. McCarthy
Department of Mathematics and Statistics, York University, Toronto, ON, Canada
Laboratory for Industrial and Applied Mathematics, Toronto, ON, Canada
Centre for Disease Modelling, York University, Toronto, ON, Canada
Fields-CQAM Mathematics for Public Health Laboratory, Toronto, ON, Canada

M. Potomkin
Department of Mathematics, University of California, Riverside, CA, 92521, USA
*Corresponding Author E-mail: mykhailp@ucr.edu

Mathematics Subject Classification (2010) 34F05, 35Q92, 92B05

1 Introduction

Cells strongly rely on the ability to efficiently transport cargo via motor proteins. Fast active transport (FAT) is required to deliver materials such as proteins, mRNA, mitochondria, vesicles, and organelles for use in a variety of cellular processes [7,8]. One of the three major means of intracellular transport is within networks of microtubules (MTs) [8]. To accommodate FAT, motor proteins “walk” along MTs and actin filaments (AFs) with their cargo forming a “superhighway” for cellular transportation [15,20,21]. Motor-protein families kinesin and dynein bind to the cellular material or cargo they carry as they move up and down the microtubule [4,8]. For a more general overview of molecular motor protein motion see review [18].

Defects in microtubules are known to exist, but the current literature has yet to clarify their impact on molecular motor-based transport [17]. Defects in active transport, particularly axonal, have been implicated in the progression of various diseases [8]. For instance, the defining characteristics of many neurodegenerative diseases such as Alzheimer’s disease and Amyotrophic Lateral Sclerosis (ALS) may be related to deficiencies in active transport within neurons [8]. One such area of need for immediate study is the scenario where the microtubule paths used by motor proteins become congested, obstructed, or defective. Hallmarks and early indicators of neurodegenerative diseases are an accumulation of organelles and proteins in the cell body or axon, which inhibits active transport [8]. Hence, understanding the nature of motor protein dynamics will provide insight in understanding the onset of these diseases and developing control strategies.

Advances in biophysical tools and imaging technology have allowed for many recent insightful *in vitro* experiments of motor protein behavior on microtubules [7, 8,17]. Motor-proteins may change directions, stop or pause briefly, increase their velocity, and also attach/detach from the microtubule [7]. Experimentally it is observed that this behavior may be attributed to the presence of MT-associated proteins [7]. Therefore, the cell’s ability to regulate active transport may be studied through tau MAP regions where motion of motor proteins is inhibited. We refer to these patches of high tau MAP concentration as defective regions due to their effects on the reduction of motor motility. We focus our study to modeling collective motor protein motility on MTs, first homogeneous and then defective.

Modeling motor protein motility on MTs has received recent theoretical attention. A one-dimensional discrete lattice model was studied in detail using a mean-field approach, including a full phase diagram for the stationary states [1, 3, 5,13,14]. The model was capable of predicting the emergence of interior layers by splitting the equilibrium density of motor proteins along the MT into two phases: low and high density. Such a co-existence corresponds to a traffic jam consisting of motor proteins translating along the MT in one direction, from the region with low density to the one with high density. In addition, a generalization of this lattice gas model has also been studied to account for local interactions between motors [12]. In particular, the effects of adjacent motors enhancing the detachment rate as well as motor crowding enhancing the frequency which motors become inactive or paused [12]. In a similar light, models featuring multiple “lanes” on a MT and

motor proteins may switch lanes have also been studied [9] or between a filament and a tube in [19]. The common feature among these lattice gas models is they follow the totally asymmetric simple exclusion process (TASEP) framework [1]. These models also feature attachment and detachment processes for motors whose stationary states are described by the theory of Langmuir dynamics [1].

In this paper, we seek to advance the current understanding of subcellular transport along microtubules with a defective region. In Section 2, we introduce a new discrete model for motor protein motility on a microtubule with a one-dimensional lattice following the TASEP paradigm and attachment/detachment dynamics. The distinctive feature of this model is that the MT consists of a defective region with decreased motor protein motility rate. From a discrete lattice formulation, we take the limit to recover the mean-field form of these equations. Next, in Section 2.3, we verify that our mean-field approximations produce results consistent with existing studies (e.g., [1, 3, 5]) before moving to the defective region case where motility will be hindered. The main analytical results are then presented in Section 2.4, where we consider examples with the domain split into two regions, fast and slow, whereas the local and boundary attachment/detachment rates are varied as parameters. From these studies we find a closed-form expression of the solution given a set of the model parameters for attachment, detachment, and boundary conditions. We then verify that the analytical solution of the mean-field model is consistent with corresponding Monte Carlo simulations of the original discrete lattice model in Section 3. We note that if one needs to consider a wide range of problem parameters, for example, in model calibration or a control problem (e.g., finding the location and width of a defective region for a desired motor distribution), Monte Carlo simulations are prohibitively time consuming as compared to a closed-form expression when available. In the Appendix, we provide a new analytical approach to the solution of the homogeneous problem, based on the analysis of the phase portrait of the corresponding system of ODEs; then we give examples of applications of the approach for specific problem parameters. Overall, this work provides a critical result for inhomogeneous MTs consisting of multiple parts with different motility properties; namely, it can be modeled as segments of homogeneous MTs linked by a matching flux condition. This greatly expands the utility of past studies that developed the theory of homogeneous MTs.

2 Mathematical Model

2.1 Discrete problem

Following the general TASEP paradigm, we construct a discrete model from first principles which generalizes previous models for homogeneous MTs to incorporate a defective region. Briefly, the TASEP paradigm states: (i) each binding site may be occupied by a maximum of one motor; (ii) motors move unidirectionally on the lattice and (iii) motors enter the lattice on the left side and exit the lattice on the right side [1]. Here we also account for the attachment and detachment of motor proteins on the MT interior as in works similar in scope focused on modeling [1, 3, 5] and experiment [16]. Another recent work has focused on stochastic modeling with the goal of revealing how motor protein and filament properties affect transport [22].

Specifically, consider a one-dimensional lattice $\{0 = x_0 < x_1 < \dots < x_M = \ell\}$, representing sites which a motor may occupy on a microtubule of length ℓ . Introduce ρ_i^n which is the probability of finding a motor at site x_i at time step n . Probabilities at each lattice site $0 \leq \rho_i^n \leq 1$ for $1 \leq i < M$ change during one time step via

$$\rho_i^{n+1} - \rho_i^n = v_{i-\frac{1}{2}} \rho_{i-1}^n (1 - \rho_i^n) - v_{i+\frac{1}{2}} \rho_i^n (1 - \rho_{i+1}^n) + \omega_A (1 - \rho_i^n) - \omega_D \rho_i^n. \quad (1)$$

The first term on the right-hand side of (1) says that the probability of finding a motor at site x_i increases due to a possible jump of a motor from site x_{i-1} to x_i provided that the following jump condition is satisfied: there is a motor at site x_{i-1} and site x_i is vacant. As it is done in previous works on one-dimensional transport of active motors along a microtubule [1, 3, 5], consider the problem in the mean-field approximation, that is, correlations are negligibly small and the probability of the jump condition is simply $\rho_{i-1}^n (1 - \rho_i^n)$. Additionally, the coefficient $v_{i-\frac{1}{2}}$ accounts for inhomogeneity of the microtubule: if the jump condition is satisfied on the interval $[x_{i-1}, x_i]$, then the jump occurs with probability (motility rate) $v_{i-\frac{1}{2}}$, and these coefficient may change from site to site. The second term on the right-hand side of (1) is similar to the first term, but accounts for the decrease in probability ρ_i^n due to a possible jump from site x_i to x_{i+1} . The third term on the right-hand side of (1) describes the interaction of the microtubule with the exterior environment: a motor from outside can attach to the microtubule at site x_i as well as a motor already occupying site x_i can detach from the microtubule. Parameters ω_A and ω_D are the corresponding attachment and detachment rates.

Stationary states of (1) solve the following system:

$$0 = v_{i-\frac{1}{2}} \rho_{i-1} (1 - \rho_i) - v_{i+\frac{1}{2}} \rho_i (1 - \rho_{i+1}) + \omega_A (1 - \rho_i) - \omega_D \rho_i. \quad (2)$$

This system is supplemented with boundary conditions corresponding to the attachment rate α at the left end and detachment rate β at the right end of the microtubule:

$$\rho_0 = \alpha \quad \text{and} \quad \rho_M = 1 - \beta. \quad (3)$$

We note here that it is assumed that boundary attachment rates have a corresponding relationship to those inside the microtubule, that is,

$$\alpha = \frac{\omega_A}{\omega_A + \omega_D} \quad \text{and} \quad \beta = \frac{\omega_D}{\omega_A + \omega_D}, \quad (4)$$

and $v_i \equiv v$, then the solution of (2)-(3) is simply a constant: $\rho \equiv \omega_A / (\omega_A + \omega_D)$. However, in practice, rates α and β are different from (4) which leads to non-trivial stationary solutions possessing interior jumps, even in the homogeneous case $v_i \equiv \text{const}$ [1, 3].

We end this subsection with another form of (2) which is helpful for understanding the continuous limit presented in Section 2.2. Introduce the following notation for the flux between sites x_{i-1} and x_i :

$$J_{i-\frac{1}{2}} = v_{i-\frac{1}{2}} \rho_{i-1} (1 - \rho_i). \quad (5)$$

Note that if one interpolates ρ_i by a smooth function $\rho(x)$ such that $\rho(x_i) = \rho_i$, then performing Taylor expansions one can verify that

$$\frac{\Delta x}{2} \rho'_{i-\frac{1}{2}} = -v_{i-\frac{1}{2}}^{-1} J_{i-\frac{1}{2}} + \rho_{i-\frac{1}{2}} (1 - \rho_{i-\frac{1}{2}}) + o(\Delta x), \quad (6)$$

where $\rho_{i-\frac{1}{2}} = \rho(x_{i-\frac{1}{2}})$, $\Delta x = x_i - x_{i-1}$, and $x_{i-\frac{1}{2}} = x_i - \frac{1}{2}\Delta x$.

Going back to definition (5), we point out that, in terms of $J_{i\pm\frac{1}{2}}$, equation (2) has the following form:

$$J_{i+\frac{1}{2}} - J_{i-\frac{1}{2}} = \omega_A(1 - \rho_i) - \omega_D\rho_i \quad (7)$$

2.2 Limiting continuous problem

We focus on the asymptotic behavior of solutions of (2)-(3) as $M \rightarrow \infty$ in the framework of the mean-field limit. Specifically, we introduce parameter $\varepsilon := \ell M^{-1} \ll 1$ (here ℓ represents the total length of microtubule) and lattice $\{x_i = i\varepsilon, i = 0, \dots, M\}$ with the distance between lattice points ε . For small ε , we approximate the solution with the continuous function $\rho_\varepsilon(x)$ defined on $0 < x < \ell$ and derived from a discrete set of unknowns ρ_i associated with the lattice points x_i , *i.e.*, $\rho_\varepsilon(x_i) = \rho_i$. Then for $\varepsilon \ll 1$, the system of algebraic equations (2) for the unknown ρ_i 's becomes a second order ordinary differential equation for unknown function $\rho_\varepsilon(x)$:

$$\partial_x \left(v(x) \left(-\frac{\varepsilon}{2} \partial_x \rho_\varepsilon + \rho_\varepsilon(1 - \rho_\varepsilon) \right) \right) = \Omega_A - (\Omega_A + \Omega_D)\rho_\varepsilon, \quad (8)$$

where $v(x)$ is the velocity the motor proteins move with at location x , and $\Omega_{A/D} = M\omega_{A/D}$ are properly rescaled attachment/detachment rates. The equalities in (3) become boundary conditions for $\rho_\varepsilon(x)$:

$$\rho_\varepsilon(0) = \alpha \quad \text{and} \quad \rho_\varepsilon(\ell) = 1 - \beta. \quad (9)$$

Remark 1 In order to obtain (8) from (2) we take the discrete-to-continuous limit $\varepsilon \rightarrow 0$. Specifically, we write both (6) and (7), which considered together are equivalent to (2), with $\Delta x = \varepsilon \ll 1$:

$$\begin{cases} \frac{\varepsilon}{2} \rho'_{i-\frac{1}{2}} = -v_{i-\frac{1}{2}}^{-1} J_{i-\frac{1}{2}} + \rho_{i-\frac{1}{2}}(1 - \rho_{i-\frac{1}{2}}) + o(\varepsilon), \\ J'_i = \Omega_A(1 - \rho_i) - \Omega_D\rho_i + o(\varepsilon). \end{cases} \quad (10)$$

We then disregard the $o(\varepsilon)$ terms and write resulting equations for all $x \in (0, \ell)$:

$$\begin{cases} \frac{\varepsilon}{2} \rho' = -v^{-1}J + \rho(1 - \rho), \\ J' = \Omega_A(1 - \rho) - \Omega_D\rho (= \Omega_A - (\Omega_A + \Omega_D)\rho). \end{cases} \quad (11)$$

Finally, we find J from the first equation of the system above and substitute it into the second equation to derive (8) for $\rho = \rho_\varepsilon$. Here both notations ρ' and $\partial_x \rho$ denote the derivative in x . It turns out that the phase portrait of system (11) of two coupled first order differential equations is the key to constructing the solutions of (8)-(9), see Appendix A.

Remark 2 Alternatively, in the case of the continuous velocity $v(x)$, this equation can be formally derived from (2) by using a Taylor expansion of a smooth function $\rho_\varepsilon(x)$ which is again obtained by interpolation of the values ρ_i on the mesh points x_i . If $v(x)$ is piecewise continuous with a finite number of jumps, then one needs to supplement equation (8), which holds inside the intervals of continuity of $v(x)$, with a continuity condition for the flux

$$J_\varepsilon(x) := v(x) \left(-\frac{\varepsilon}{2} \rho'_\varepsilon + \rho_\varepsilon(1 - \rho_\varepsilon) \right).$$

One can also consider (8) in the distributional sense. Then using the definition of $J_\varepsilon(x)$, the integration of (8) in x , and the absolute continuity of integrals together imply the continuity of flux $J_\varepsilon(x)$:

$$\begin{aligned} J_\varepsilon(x) &= J_\varepsilon(0) + \int_0^x [\Omega_A - (\Omega_A + \Omega_D)\rho_\varepsilon(s)] ds \\ &= J_\varepsilon(0) + \Omega_A x - (\Omega_A + \Omega_D) \int_0^x \rho_\varepsilon(s) ds. \end{aligned} \quad (12)$$

In what follows below, we assume that for all $\varepsilon > 0$, there exists unique smooth solution $0 \leq \rho_\varepsilon(x) < 1$ which solves (8) and satisfies the boundary conditions (9). Moreover, there exists a piecewise smooth function $\rho_0(x)$, referred to as the ‘‘outer solution’’, such that

$$\lim_{\varepsilon \rightarrow 0} \rho_\varepsilon(x) = \rho_0(x), \quad \text{for all } 0 \leq x \leq \ell. \quad (13)$$

By calling $\rho_0(x)$ the outer solution we stick to the standard terminology of singularly perturbed ordinary differential equations [6]. While the outer solution $\rho_0(x)$ is the pointwise limit of $\rho_\varepsilon(x)$ for $0 \leq x \leq \ell$, it does not approximate the exact solution $\rho_\varepsilon(x)$ uniformly on $0 \leq x \leq \ell$. Specifically, the outer solution $\rho_0(x)$ approximates $\rho_\varepsilon(x)$ poorly in the vicinity of the jumps $\{x_J\}$. To make the approximation uniform, one takes into account boundary layer terms of the form $\rho_{\text{corrector}}(x) = Y((x - x_J)/\varepsilon)$ whose distinguishing feature is that its slope, derivative in x , is of the order of ε^{-1} . Observe also that, even though $\rho_0(0) = \alpha$ and $\rho_0(\ell) = 1 - \beta$, it is possible that the outer solution $\rho_0(x)$ does not satisfy the boundary condition in the following sense: either $\lim_{x \rightarrow 0^+} \rho_0(x) \neq \alpha$ or $\lim_{x \rightarrow \ell^-} \rho_0(x) \neq 1 - \beta$.

Remark 3 We note that (1) possesses a unique constant solution $\rho_i \equiv \Omega_A/(\Omega_A + \Omega_D)$. In what follows, we are interested in regimes where jamming can occur and, thus, for the sake of simplicity we restrict ourselves to the case when the attachment rate exceeds the detachment rate, that is, $\Omega_A > \Omega_D$. This implies that the constant solution of (1) is greater than $1/2$.

2.3 Homogeneous microtubule

Consider a constant motor protein motility rate $v(x)$, representing a homogeneous microtubule, that is, $v_i \equiv v_0$. The solution in the homogeneous case has been studied previously (e.g., [1,2,3]). In this case, (8) reduces to

$$v_0 \partial_x \left(-\frac{\varepsilon}{2} \partial_x \rho_\varepsilon + \rho_\varepsilon(1 - \rho_\varepsilon) \right) = \Omega_A - (\Omega_A + \Omega_D)\rho_\varepsilon, \quad 0 < x < \ell, \quad (14)$$

$$\rho_\varepsilon(0) = \alpha, \quad \rho_\varepsilon(\ell) = 1 - \beta. \quad (15)$$

Recall that ℓ is the length of a microtubule.

Equation (14) is a second order nonlinear ODE. If one formally passes to the limit $\varepsilon \rightarrow 0$ in (14), then the term with the second derivative of ρ_ε vanishes and this equation becomes first order where the solution cannot, in general, satisfy both

boundary conditions in (15) as the boundary value problem is overdetermined. To describe the limiting solution, $\lim_{\varepsilon \rightarrow 0} \rho_\varepsilon(x)$, we introduce an auxiliary function $g(x; s, a)$, which is the solution of the initial value problem of the first order obtained from the formal limit as $\varepsilon \rightarrow 0$ in (14):

$$\begin{cases} v_0(1-2g)\partial_x g = \Omega_A - (\Omega_A + \Omega_D)g, \\ g(x=s; s, a) = a. \end{cases} \quad (16)$$

In other words, function $\rho_0(x) := g(x; s, a)$ is the smooth outer solution subject to a single boundary condition (or, equivalently, initial condition): $\rho_0|_{x=s} = a$. Equation (16) can be solved in an explicit form in terms of special functions (see [3]).

Note that initial value problem (16) is not well-posed for $a = 0.5$. If $a = 0.5$, then there is no solution for $x > s$, and for $x < s$ we define g as the function solving the differential equation in (16) subject to the following condition:

$$\lim_{x \rightarrow s} g(x; s, 0.5) = 0.5 \text{ and } g(x; s, 0.5) > 0.5 \text{ for all } x < s. \quad (17)$$

In other words, for the initial condition with $a = 0.5$, equation (16) admits two solutions for $x < s$: one solution is less than 0.5, another one is above 0.5, and to describe the outer solution $\rho_0(x)$ we will need restrict our consideration to the upper one (the upper solution is stable in a certain sense, see Appendix A).

Function $g(x; s, a)$ is not necessarily defined globally, for all x . For example, consider $x \geq s$, then the solution exists on the interval $(s, s + x_a)$ for some $x_a > 0$ and at $x = s + x_a$ the slope of g becomes unbounded. For example, if $a < 0.5$, then the value of x_a can be found from the condition $g(s + x_a; s, a) = 0.5$ which can be written as

$$x_a = \int_a^{0.5} \frac{dg}{v(g)} = \int_a^{0.5} \frac{v_0(1-2g)dg}{\Omega_A - (\Omega_A + \Omega_D)g}, \quad (18)$$

where function $v(g)$ is introduced in such a way that the differential equation from (16) is equivalent to $\partial_x g = v(g)$. One can compute the integral on the right-hand side of (18) to obtain an analytic formula for x_a :

$$x_a = v_0 \frac{\Omega_A - \Omega_D}{(\Omega_A + \Omega_D)^2} \log \frac{\Omega_A - \Omega_D}{2(\Omega_A - a(\Omega_A + \Omega_D))} + v_0 \frac{1-2a}{\Omega_A + \Omega_D}. \quad (19)$$

The following theorem gives an explicit formula for the limiting solution of the (14)-(15) as $\varepsilon \rightarrow 0$.

Theorem 1 Define $\rho_0(x) := \lim_{\varepsilon \rightarrow 0} \rho_\varepsilon(x)$ for $0 \leq x \leq \ell$ and ρ_ε solving (14)-(15). Then

$$\rho_0(x) = \begin{cases} \alpha, & x = 0, \\ g(x; 0, \alpha), & 0 < x < \max\{0, x_J\}, \\ g(x; \ell, \max\{0.5, 1 - \beta\}), & \max\{0, x_J\} < x < \ell, \\ 1 - \beta, & x = \ell. \end{cases} \quad (20)$$

If $\alpha \geq 1/2$, then $x_J = 0$. If $\alpha < 1/2$, then x_J is determined by

$$x_J := \min \{x \geq 0 \mid g(x; 0, \alpha) + g(x; \ell, \max\{0.5, 1 - \beta\}) \leq 1\}. \quad (21)$$

The result of this theorem is consistent with previous works where the system (14)-(15) was studied (e.g., see [5, 9, 12]). We relegate the proof of this theorem and examples of the application of the representation formula (20) to Appendix A.

Remark 4 The point x_J , if $0 < x_J < \ell$, is the location of the interior jump, that is, the outer solution $\rho_0(x)$ is a smooth solution of the differential equation from (16) on intervals $(0, x_J)$ and (x_J, ℓ) and it has one jump inside $(0, \ell)$ at $x = x_J$. The value of x_J can also be found via numerical simulations of the following equation

$$g(x_J; 0, \alpha) + g(x_J; \ell, \max\{0.5, 1 - \beta\}) = 1. \quad (22)$$

This equation is equivalent to the continuity of fluxes $J_0 = \rho_0(1 - \rho_0)$ at the point of the jump of the outer solution $\rho_0 = \rho_0(x)$:

$$v_0 \rho_\alpha (1 - \rho_\alpha)|_{x \rightarrow x_J^-} = v_0 \rho_\beta (1 - \rho_\beta)|_{x \rightarrow x_J^+}, \quad (23)$$

where $\rho_\alpha(x) = g(x; 0, \alpha)$ and $\rho_\beta(x) = g(x; \ell, \max\{0.5, 1 - \beta\})$.

Remark 5 If one varies boundary conditions (15), then the outer solution $\rho_0(x)$ may stay unchanged (except values at $x = 0$ and $x = \ell$) for wide range of parameters α and β . For example, denote $\rho_\beta(x) := g(x, \ell, \max\{0.5, 1 - \beta\})$. Theorem 1 implies that outer solution $\rho_0(x)$ coincides with $\rho_\beta(x)$ on the interval $0 < x < 1$ for the following range of α :

$$1 - \rho_\beta(0) \leq \alpha \leq 1. \quad (24)$$

Once α becomes smaller than the lower limit, $1 - \rho_\beta(0)$, an interior jump appears in the outer solution $\rho_0(x)$.

The following corollary is important for the study of inhomogeneous microtubules in Section 2.4.

Corollary 1 *Assume $\alpha \geq 1/2$ or*

$$\int_0^{0.5} \frac{v_0(1 - 2\rho)}{\Omega_A - (\Omega_A + \Omega_D)\rho} d\rho \leq \ell. \quad (25)$$

Then

- (i) $\lim_{x \rightarrow \ell^-} \rho_0(x) = \max\{0.5, 1 - \beta\}$.
- (ii) If $\beta < 1/2$, then $\rho_0(x)$ is continuous at $x = \ell$, that is, $\lim_{x \rightarrow \ell^-} \rho_0(x) = \rho_0(0) = 1 - \beta$.
- (iii) If $\alpha \geq 1/2$, then there is no interior jump, that is, $x_J \leq 0$.
- (iv) If $0 < x_J < \ell$, then $\alpha < 1/2$ and $\lim_{x \rightarrow 0^+} \rho_0(x) = \alpha$ (that is, $\rho_0(x)$ is continuous at $x = 0$).

Condition (25) excludes the case of low density solutions, that is, we exclude outer solutions of the form: $\rho_0(x) < 0.5$ for all $x \in [0, \ell)$. This regime is not consistent with jamming, which is the focus of this work. In other words, condition (25) imposes that the ‘‘left’’ part of solution, $g(x; 0, \alpha)$, cannot be extended to entire interval $[0, \ell)$. The reason we would like to impose this condition below in the inhomogeneous case is because we then focus on cases when regions with high densities emerge, and thus traffic jams in motor transport are possible. By direct integration, condition (25) can be written as

$$\frac{v_0}{\Omega_A + \Omega_D} \left[1 - \frac{\Omega_A - \Omega_D}{\Omega_A + \Omega_D} \log \left(\frac{2}{\Omega_A - \Omega_D} \right) \right] \leq \ell. \quad (26)$$

2.4 Inhomogeneous microtubule

In this section, we consider a non-constant motility rate $v(x)$. Biologically, it corresponds to an inhomogeneous microtubule with different motor protein mobilities in different regions of the microtubule. Without loss of generality, we take $\ell = 1$. We restrict ourselves to the case

$$v(x) = \begin{cases} v_L, & 0 \leq x \leq x_0, \\ v_R, & x_0 < x \leq 1. \end{cases} \quad (27)$$

This case may be considered as two coupled homogeneous microtubules meeting at interface $x = x_0$ with coupling through the continuity of densities and fluxes. Specifically, we have the following system of equations:

$$v_L \partial_x \left[\left(-\frac{\varepsilon}{2} \rho'_\varepsilon + \rho_\varepsilon (1 - \rho_\varepsilon) \right) \right] = \Omega_A - (\Omega_A + \Omega_D) \rho_\varepsilon, \quad 0 < x < x_0, \quad (28)$$

$$v_R \partial_x \left[\left(-\frac{\varepsilon}{2} \rho'_\varepsilon + \rho_\varepsilon (1 - \rho_\varepsilon) \right) \right] = \Omega_A - (\Omega_A + \Omega_D) \rho_\varepsilon, \quad x_0 < x < 1, \quad (29)$$

and two coupling conditions:

(1) continuity of $\rho_\varepsilon(x)$ at x_0 :

$$\rho_\varepsilon(x_0^-) = \rho_\varepsilon(x_0^+) =: \rho_\varepsilon. \quad (30)$$

(2) continuity of flux $J_\varepsilon(x)$ at x_0 :

$$v_L \left(-\frac{\varepsilon}{2} \rho'_\varepsilon(x_0^-) + \rho_\varepsilon(1 - \rho_\varepsilon) \right) = v_R \left(-\frac{\varepsilon}{2} \rho'_\varepsilon(x_0^+) + \rho_\varepsilon(1 - \rho_\varepsilon) \right). \quad (31)$$

The outer solution $\rho_0(x) = \lim_{\varepsilon \rightarrow 0} \rho_\varepsilon(x)$ is not necessarily continuous, nevertheless due to (12) it satisfies the flux continuity condition:

$$v_L \rho_0(1 - \rho_0) \Big|_{x \rightarrow x_0^-} = v_R \rho_0(1 - \rho_0) \Big|_{x \rightarrow x_0^+}. \quad (32)$$

Remark 6 By looking at the system (28)-(29) one may think that the case of inhomogeneous $v(x)$ is equivalent to the case of inhomogeneous attachment/detachment rates but with constant motility rates $v(x) \equiv 1$:

$$\partial_x \left(-\frac{\varepsilon}{2} \rho'_\varepsilon + \rho_\varepsilon (1 - \rho_\varepsilon) \right) = \Omega_A(x) - (\Omega_A(x) + \Omega_D(x)) \rho_\varepsilon \quad (33)$$

with attachment/detachment rates $\Omega_A(x)$ and $\Omega_D(x)$ are Ω_A/v_L and Ω_D/v_L inside the left half of the microtubules, $x < x_0$, and Ω_A/v_R and Ω_D/v_R inside the right half, $x > x_0$. For differential equation (33), from the continuity of $\rho_\varepsilon(x)$ and $J_\varepsilon(x)$, one concludes that ρ_ε is necessarily continuously differentiable, whereas the solution of (28)-(29) possesses a discontinuous derivative at x_0 for $v_L \neq v_R$ which follows from (31) and is written as

$$\rho'_\varepsilon(x_0^+) - \rho'_\varepsilon(x_0^-) = \frac{2}{\varepsilon v_R v_L (v_R - v_L)} J_\varepsilon(x_0). \quad (34)$$

Therefore, problems for inhomogeneous $v(x)$ and inhomogeneous $\Omega_{A,D}(x)$ are not equivalent.

By analogy with function g from (16) in the case of homogeneous microtubules, we introduce $g_L(x; s_L, a_L)$ and $g_R(x; s_R, a_R)$ as solutions of the following initial value problems:

$$\begin{cases} v_L(1 - 2g_L)\partial_x g_L = \Omega_A - (\Omega_A + \Omega_D)g_L, & g_L(s_L; s_L, a_L) = a_L, \\ v_R(1 - 2g_R)\partial_x g_R = \Omega_A - (\Omega_A + \Omega_D)g_R, & g_R(s_R; s_R, a_R) = a_R. \end{cases} \quad (35)$$

In what follows we consider separately two cases:

- (i) *fast - slow microtubule*: $v_L > v_R$,
- (ii) *slow - fast microtubule*: $v_R > v_L$.

Before we formulate our main result for these two cases, we note that the difficulty in the determination of the outer solution $\rho_0(x)$ is finding the value of ρ_0 at the interface, $A := \rho_0(x_0)$. Once A is found, one can use Theorem 1 to restore $\rho_0(x)$ in both intervals $[0, x_0]$ and $[x_0, 1]$.

Theorem 2 *Consider $v_L > v_R$ and assume that condition (25) holds with $v_0 = v_L$ and $\ell = x_0$. Let $\rho_0(x)$ be the outer solution of system (28)-(29) equipped with coupling conditions (30)-(31). Then function $\rho_0(x)$ has a jump at $x = x_0$ and is given by*

$$\rho_0(x) = \begin{cases} \alpha, & x = 0, \\ g_L(x; 0, \alpha), & 0 < x < \max\{0, x_J\}, \\ g_L(x; x_0, A), & \max\{0, x_J\} < x \leq x_0, \\ g_R(x; 1, \max\{0.5, 1 - \beta\}), & x_0 < x < 1, \\ 1 - \beta, & x = 1, \end{cases} \quad (36)$$

where x_J is determined from the continuity of fluxes:

$$g_L(x_J; 0, \alpha) + g_L(x_J; x_0, A) = 1, \quad (37)$$

and $A = \left(v_L + \sqrt{v_L^2 - 4J_R^2} \right) / (2v_L)$ where $J_R = v_R g_R(1 - g_R)$ with

$$g_R := g_R(x_0; 1, \max\{0.5, 1 - \beta\}).$$

Proof First, we show that the outer solution $\rho_0(x)$ has a jump at $x = x_0$. Indeed, from continuity of fluxes (31) with $\rho_\varepsilon(x_0) = A + o(1)$ we get:

$$v_L \rho'_\varepsilon(x_0^-) = v_R \rho'_\varepsilon(x_0^+) + \frac{v_L - v_R}{2\varepsilon} A(1 - A) + o\left(\frac{1}{\varepsilon}\right). \quad (38)$$

Since A is strictly between 0 and 1, we find that one of the derivatives (either the left or right one) is of the order ε^{-1} corresponding to a jump.

Next, denote the limits of the outer solution from the left and right at x_0 by

$$A_L := \rho_0|_{x \rightarrow x_0^-} \quad \text{and} \quad A_R := \rho_0|_{x \rightarrow x_0^+}.$$

Then the continuity of fluxes (32) is written as $v_L A_L(1 - A_L) = v_R A_R(1 - A_R)$, and since $v_L > v_R$ we have $A_L(1 - A_L) < 1/4$. By applying Corollary 1 (ii) we find $A = A_L > 0.5$ and thus, there is no jump from the left at x_0 . Then, following Corollary 1 (iii), there is no interior jump, and $\rho_0(x)$ in interval $[x_0, 1]$ is determined by Corollary 1 (i), which is a boundary condition for $\rho_0(x)$ at $x_0 = 1$.

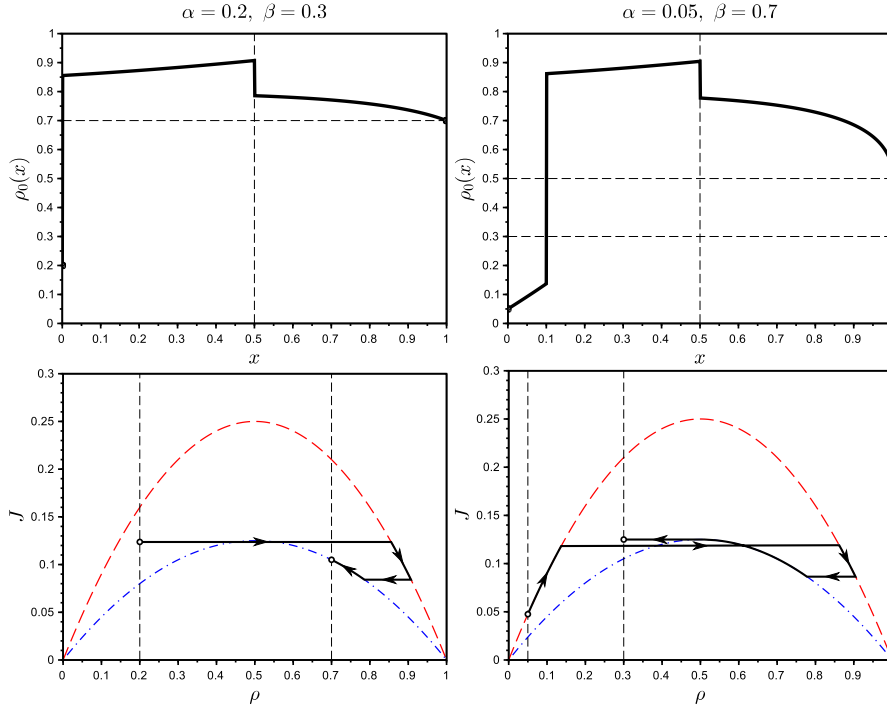


Fig. 1 Examples 1 & 2 for inhomogeneous microtubulus. The upper row depicts plots of outer solutions $\rho_0(x)$. The lower row depicts solutions as trajectories in the (ρ, J) -plane; note that these trajectories are continuous in J and have discontinuities (jumps) in ρ . Red (lower) and blue (upper) dashed lines are arcs $J = v_R \rho(1 - \rho)$ and $J = v_L \rho(1 - \rho)$, respectively.

Specifically, by Theorem 1 we have $\rho_0(x) = g_R(x; 1, \max\{0.5, 1 - \beta\})$ for $x_0 < x < 1$. Then $A_R = g_R := g_R(x_0; 1, \max\{0.5, 1 - \beta\})$ and A is the solution of the quadratic equation $v_L A(1 - A) = v_R A_R(1 - A_R)$, which is strictly greater than 0.5. Thus, we found A , and the expression for $\rho_0(x)$ in $[0, x_0]$ is found by using the representation formula (20) from Theorem 1. \square

Next, we illustrate formula (36) of Theorem 2 by the following two examples with $x_0 = 0.5$, $v_L = 1.0$, $v_R = 0.5$, $\Omega_A = 0.8$ and $\Omega_D = 0.2$.

Example 1. $\alpha = 0.2$ and $\beta = 0.3$.

$$\rho_0(x) = \begin{cases} 0.2, & x = 0, \\ g_L(x; 0.5, 0.907), & 0 < x \leq 0.5, \quad (A = 0.5(1 \pm \sqrt{1 - 4J_R}) \approx 0.907) \\ g_R(x; 1.0, 0.7), & 0.5 < x \leq 1.0. \end{cases}$$

Example 2. $\alpha = 0.05$ and $\beta = 0.7$.

$$\rho_0(x) = \begin{cases} g_L(x; 0.0, 0.05), & 0 \leq x < x_J, \quad (x_J \approx 0.101) \\ g_L(x; 0.5, 0.904), & x_J < x \leq 0.5, \\ g_R(x; 1.0, 0.5+), & 0.5 < x < 1.0, \quad (A \approx 0.904) \\ 0.3, & x = 1.0. \end{cases}$$

Solutions from Examples 1 and 2 are depicted in Fig. 1. The main difference between Examples 1 and 2 is that in Example 2 there is an interior jump in the left sub-interval $(0, 0.5)$, while the solution in Example 1 does not possess a jump in neither of the two sub-intervals, left $(0, 0.5)$ and right $(0.5, 1)$ (or, equivalently, $x_J = 0$ in (36) for Example 1).

Theorem 3 Consider $v_R > v_L$ and assume condition (25) holds with both $v_0 = v_L$, $\ell = x_0$ and $v_0 = v_R$, $\ell = 1 - x_0$. Let $\rho_0(x)$ be the outer solution of system (28)-(29) equipped with coupling conditions (30)-(31). Denote also

$$\hat{A}_R := g_R(x_0; 1, \max\{0.5, 1 - \beta\}). \quad (39)$$

Then

$$A = \begin{cases} \frac{1}{2} - \sqrt{\frac{1}{4} - \frac{v_L}{4v_R}}, & v_R \hat{A}_R (1 - \hat{A}_R) > 0.25v_L, \\ \frac{1}{2} + \sqrt{\frac{1}{4} - \frac{v_R}{v_L} \hat{A}_R (1 - \hat{A}_R)}, & v_R \hat{A}_R (1 - \hat{A}_R) \leq 0.25v_L, \end{cases} \quad (40)$$

and function $\rho_0(x)$ is given by

$$\rho_0(x) = \begin{cases} \alpha, & x = 0, \\ g_L(x; 0, \alpha), & 0 < x < \max\{0, x_J^{(L)}\}, \\ g_L(x; x_0, \max\{A, 0.5\}), & \max\{0, x_J^{(L)}\} \leq x < x_0, \\ g_R(x; x_0, \min\{A, 0.5\}), & x_0 \leq x \leq x_J^{(R)}, \\ g_R(x; 1, \max\{0.5, 1 - \beta\}), & x_J^{(R)} < x < 1, \\ 1 - \beta, & x = 1. \end{cases} \quad (41)$$

Here $x_J^{(L)}$ and $x_J^{(R)}$ are determined from the continuity of fluxes:

$$\begin{aligned} g_L(x_J^{(L)}; 0, \alpha) + g_L(x_J^{(L)}; x_0, \max\{A, 0.5\}) &= 1, \\ g_R(x_J^{(R)}; x_0, \min\{A, 0.5\}) + g_R(x_J^{(R)}; 1, \max\{0.5, 1 - \beta\}) &= 1. \end{aligned}$$

Proof As in the proof of Theorem 2, introduce $A_L := \rho_0|_{x \rightarrow x_0^-}$ and $A_R := \rho_0|_{x \rightarrow x_0^+}$. Then continuity of fluxes at x_0 reads

$$v_L A_L (1 - A_L) = v_R A_R (1 - A_R). \quad (42)$$

By Corollary 1 (i) we get $A_L \geq 0.5$. Next, we consider two cases. If

$$\frac{v_R}{v_L} \hat{A}_R (1 - \hat{A}_R) \leq 1/4,$$

then $A_R = \hat{A}_R$ and $A_L \geq 0.5$ solves (42), that is,

$$A = A_L = \frac{1}{2} + \sqrt{\frac{1}{4} - \frac{v_R}{v_L} \hat{A}_R (1 - \hat{A}_R)}.$$

If $\frac{v_R}{v_L} \hat{A}_R (1 - \hat{A}_R) > 1/4$, then $\rho_0(x)$ does not coincide with $g_R(x; 1, \max\{0.5, 1 - \beta\})$ on the entire interval $(x_0, 1)$, there is an interior jump at $x_0 < x_J^{(R)} < 1$ and by Corollary 1 (iii) and (iv), $A_R < 1/2$ and $A = A_R$. Then $A_L = 1/2$ and $\rho_0(x)$ on intervals $(0, x_0)$ and $(x_0, 1)$ is found by (20). \square

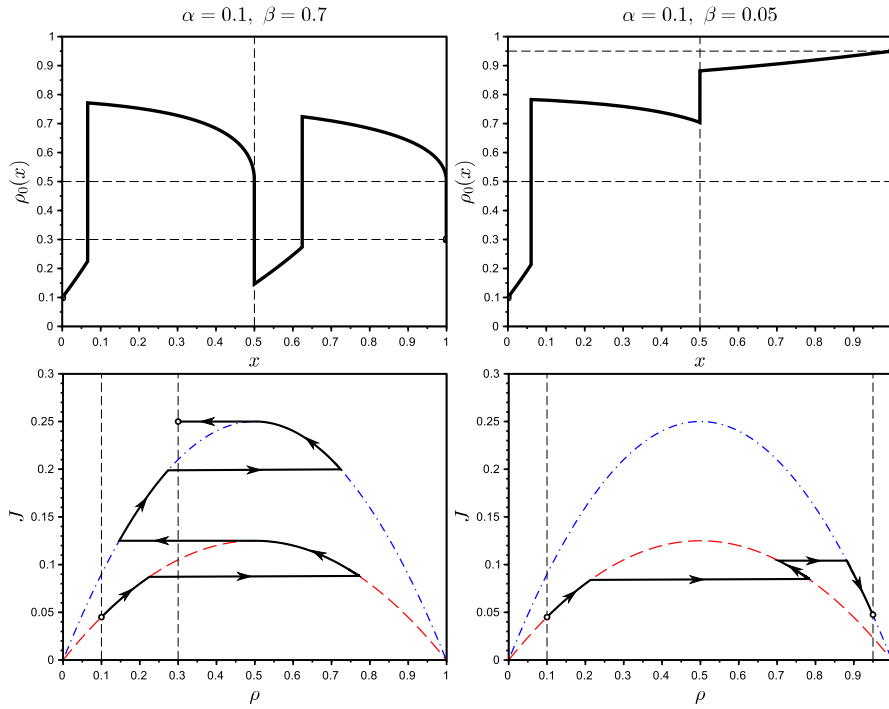


Fig. 2 Examples 3 & 4 for an inhomogeneous microtubule. The upper row depicts plots of outer solutions $\rho_0(x)$. The lower row depicts solutions as trajectories in (ρ, J) plane, red (lower) and blue (upper) dashed lines are arcs $J = v_L \rho(1 - \rho)$ and $J = v_R \rho(1 - \rho)$, respectively.

Next we illustrate formula (41) by two examples with $v_R > v_L$. Namely, set $v_L = 0.5$ and $v_R = 1.0$ and consider $x_0 = 0.5$, $\Omega_A = 0.8$ and $\Omega_D = 0.2$.

Example 3. $\alpha = 0.1$ and $\beta = 0.7$.

$$\rho_0(x) = \begin{cases} g_L(x; 0.0, 0.1), & 0 \leq x < x_J^{(L)}, (x_J^{(L)} \approx 0.097) \\ g_L(x; 0.5, 0.5+), & x_J^{(L)} < x < 0.5, \\ g_R(x; 0.5, A), & 0.5 \leq x < x_J^{(R)}, (A = \frac{1}{2}(1 - \frac{1}{\sqrt{2}}), x_J^{(R)} \approx 0.624) \\ g_R(x; 1.0, 0.5+), & x_J^{(R)} < x < 1.0, \\ 0.3, & x = 1.0. \end{cases}$$

Example 4. $\alpha = 0.1$ and $\beta = 0.05$.

$$\rho_0(x) = \begin{cases} g_L(x; 0.0, 0.1), & 0 \leq x < x_J^{(L)}, (x_J^{(L)} \approx 0.09) \\ g_L(x; 0.5, A), & x_J^{(L)} \leq x \leq 0.5, (A \approx 0.703) \\ g_R(x; 1.0, 0.95), & 0.5 < x \leq 1. \end{cases}$$

Solutions from Examples 3 and 4 are depicted in Fig. 2. These two examples illustrate two possibilities for slow-fast microtubules: when $\rho_0(x)$ is continuous from the right at x_0 (Example 3) and when it is continuous from the left at x_0 (Example 4).

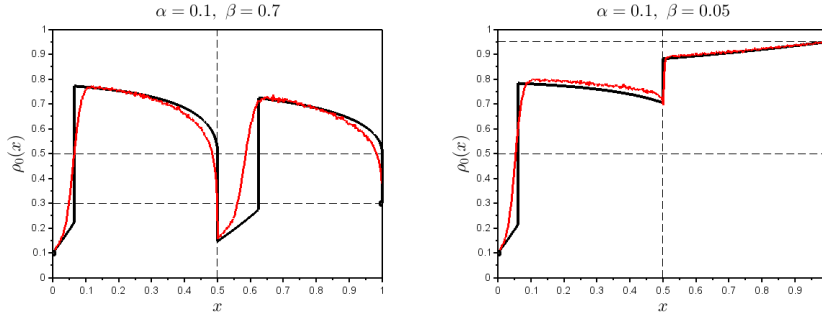


Fig. 3 Examples 3 & 4 are simulated with $R = 10^4$ realizations of the lattice model, described in Section 3. Simulations use the same parameters as Examples 3 & 4 for inhomogeneous microtubules above (analytical solution is solid black line; see also Figure 2). We see a strong quantitative agreement between the Monte Carlo (red) and analytical (black) solutions.

3 Monte Carlo Simulations

We now show that the results from Section 2.4 involving the mean-field continuous model in the inhomogeneous case are consistent with those from Monte Carlo simulations. To this end, we return to the discrete problem (2)-(3) with $M = 500$ lattice sites. We perform $R = 10^4$ realizations and compare the resulting discrete densities with the continuum equation (8) as $\varepsilon \rightarrow 0$, computed by representation formulas from Theorem 2 and 3.

Specifically, we adapt a similar algorithm to the one in [1]. In each realization $r = 1, \dots, R$ we consider tuple $\{\nu^{(n)}(i)\}$ where n stands for the iteration step number and $\nu^{(n)}(i) = 1$ if the i th site is occupied at the n th iteration step and $\nu^{(n)}(i) = 0$, if otherwise. Initially, microtubule is empty, i.e., $\nu^{(0)}(i) = 0$ for $i = 1, \dots, M$. For each time step, $n = 1, \dots, N$ discrete dynamics of $\{\nu^{(n)}(i)\}_{i=1}^M$ is described by the following procedure:

1. Choose randomly site i (all sites are equiprobable).
2. If $i = 1$ and $\nu^{(n)}(1) = 0$, then $\nu^{(n+1)}(1) = 1$ with probability α .
3. If $i = M$ and $\nu^{(n)}(M) = 1$, then $\nu^{(n+1)}(M) = 0$ with probability β .
4. If $1 < i < M$, then
 - if $\nu^{(n)}(i) = 0$, then $\nu^{(n+1)}(i) = 1$ and $\nu^{(n+1)}(i-1) = 0$ with probability $v_{i-\frac{1}{2}}$ provided that $\nu^{(n)}(i-1) = 1$;
 - if $\nu^{(n)}(i) = 1$, then $\nu^{(n+1)}(i) = 0$ and $\nu^{(n+1)}(i+1) = 1$ with probability $v_{i+\frac{1}{2}}$ provided that $\nu^{(n)}(i+1) = 0$.
5. If $1 < i < M$, then
 - if $\nu^{(n+1)}(i) = 1$ after step 4, then let $\nu^{(n+1)}(i) = 0$ with probability ω_d ;
 - if $\nu^{(n+1)}(i) = 0$ after step 4, then let $\nu^{(n+1)}(i) = 1$ with probability ω_a .

Finally, after running N steps and R realizations, we assign $\rho_i^{\text{MCS}} := \langle \nu_i^{(N)} \rangle_r$.

Monte Carlo simulations are in very good agreement with the outer solutions derived in Section 2.4. Specifically, results of Monte Carlo simulations corresponding to Example 3 and 4 from Section 2.4 are depicted in Fig. 3; one can see agreement between histograms obtained from Monte Carlo simulations (red) and

analytical solutions (black). Observe that number of realizations R and number of iteration steps N needed to reach equilibrium are critical for recovering the sharp transitions observed near the interface of the inhomogeneous microtubule. For Monte Carlo histograms in Fig. 3, we were to take $N = 2.5 \cdot 10^6$ time steps in order to guarantee that a transient solution has reached equilibrium for each of $R = 10^4$ realizations. The large numbers for both realizations and iteration steps lead to the observation that the reproduction of equilibrium profiles (solutions) in Examples 1-4 by Monte Carlo simulations to be very time consuming, whereas Theorems 2 and 3 give explicit formulas which require only numerical integration of at most four ODEs for the auxiliary functions $g(x; s, a)$.

4 Discussion

In this work, we present a mathematical model to describe dynamics of motor proteins on microtubules. Using methods from asymptotic analysis, we provide closed-form expressions for motor protein density solutions. We also provide verification of the results of mathematical analysis by Monte Carlo simulation with the discrete MT model. The mathematical model may serve as a convenient framework for studying experimental data. Even more, the modeling and analysis may assist in inferring *in vivo* dynamics where biophysical imaging is limited in the crowded cellular environments. It is also important to note that the model presented herein is consistent with prior theoretical results for the homogeneous case (e.g., [1, 3, 5]).

The model approach developed herein provides additional advantages over the prior approach of Frey et al. [12] and others [13, 14] while remaining faithful in the homogeneous case. Most notably, the model is developed to study inhomogeneous regimes where large density profiles can result in the emergence of internal boundary layers. Beyond the obvious application to motor protein dynamics along a microtubule, this also provides insight into traffic flow problems. The PDE governing the density of cars has a similar form to the equation governing the density of motor proteins here. This work also provides an additional example of the power of analyzing discrete ODE model systems by passing to the limit and obtaining a mean-field PDE.

What made this work challenging is that *a priori* initial data cannot predict regions of low or high density. Even within the Monte Carlo simulations we observe that they must be run for a significant length of time to capture all the feature of the solutions (e.g, interior boundary layers, sharp transitions etc.). An additional challenge lies in experimental verification given the current state of technology. Once imaging technology improves combined with advancements in biophysical knowledge, the theory developed in this manuscript can be rigorously tested experimentally both *in vitro* and *in vivo*. This will be crucial in verifying model parameter regimes corresponding to biologically realistic results.

This work lays the foundation for future work in understanding inhibited transport along microtubules. The model we present may be augmented to account for more biological realism in describing motor protein dynamics and intracellular transport. Realistically there are several “lanes” on these MTs which motor proteins move laterally and they may switch lanes. Similarly, motor proteins may also change directions when encountering patches [7]. Furthermore, transport takes place on highly complex 3-dimensional networks of many MTs and AFs. Hence

modeling the intersections between MTs would be of interest as well as analyzing the composite density profiles using the analysis presented in this work. In addition, the cargo transported to and from the cell nucleus and cell wall is carried by motor proteins [8,4] and the given model may be augmented to account for this cargo. We also note that motor proteins transfer from MT to MT within the cell, and the model as well as analysis developed here may serve as a foundation for this study.

Overall, the model for an inhomogeneous microtubule presented here can inform motor protein dynamics in *rough* regimes where transport properties are not consistent along given trajectories. This will ultimately lay the groundwork for fundamental understanding of the onset of neurodegenerative diseases. The inhomogeneous microtubule model may be used to investigate how one can control transport properties of motor proteins in high density regimes along microtubules. Given the structure of a microtubule, can one devise conditions so that the equilibrium solution contains no high density regimes (jams) by understanding or imposing defects along its surface? Also, given a distribution of inhomogeneous regions ($N > 2$) on a microtubule can we predict the equilibrium solution? The answers to these questions may be the source of further investigation in a future work.

Acknowledgements The work of SR was supported by the Cleveland State University Office of Research through a Faculty Research Development Grant.

References

1. Parmeggiani, A., Franosch, T. and Frey, E., 2003. *Phase coexistence in driven one-dimensional transport*. Physical review letters, **90**, p.086601.
2. Popkov, V., Rákos, A., Willmann, R.D., Kolomeisky, A.B. and Schütz, G.M., 2003. *Localization of shocks in driven diffusive systems without particle number conservation*. Physical Review E, **67**, p.066117.
3. Parmeggiani, A., Franosch, T. and Frey, E., 2004. *Totally asymmetric simple exclusion process with Langmuir kinetics*. Physical Review E, **70**, p.046101.
4. Gross, S. P., Vershinin, M. and Shubeita G. T., 2007. *Cargo transport: Two motors are sometimes better than one*. Current Biology, **17**, R478-R486.
5. Reese, L., Melbinger, A. and Frey, E., 2011. *Crowding of molecular motors determines microtubule depolymerization*. Biophysical Journal, **101** p. 2190-2200.
6. M. H. Holmes, *Introduction to Perturbation Methods*, 2nd edition. Texts in Applied Mathematics, 20. Springer, New York, 2013. xviii+436 pp.
7. Ross, J. L., Ali, M. Y. and Warshaw, D. M., 2008. *Cargo transport: molecular motors navigate a complex cytoskeleton* Current Opinion in Cell Biology, **20** p. 41-47.
8. Lakadamyali, M., 2014. *Navigating the cell: how motors overcome roadblocks and traffic jams to efficiently transport cargo* Phys. Chem. Chem. Phys., **16** p. 5907.
9. Reichenbach, T., Frey, E. and Franosch, T., 2007. *Traffic jams induced by rare switching events in two-lane transport* New Journal of Physics, **9** p. 159.
10. Tan, R., Lam, A.J., Tan, T., Han, J., Nowakowski, D.W., Vershinin, M., Simo, S., Ori-McKenney, K.M. and McKenney, R.J., 2019. *Microtubules gate tau condensation to spatially regulate microtubule functions*. Nature cell biology, **21**(9), pp.1078-1085.
11. Oelz, D. and Mogilner, A., 2016. *A drift-diffusion model for molecular motor transport in anisotropic filament bundles*. Discrete and Continuous Dynamical Systems, **36**:8 p. 4553-4567.
12. Rank, M. and Frey, E., 2018. *Crowding and pausing strongly affect dynamics of kinesin-1 motors along microtubules*. Biophysical journal, **115**(6), 1068-1081.

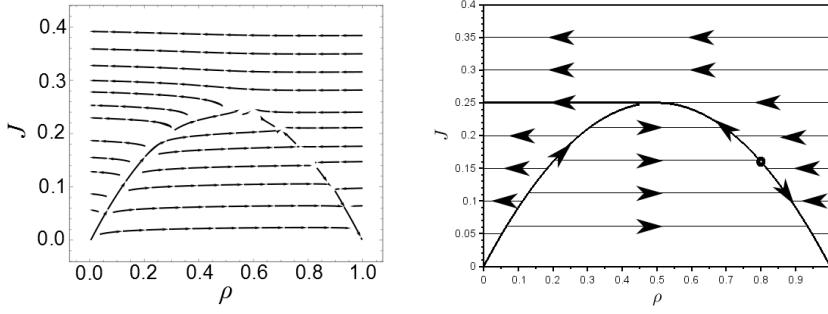


Fig. 4 Left: Phase portrait for (43) with $\varepsilon = 0.01$, $\Omega_A = 0.7$ and $\Omega_D = 0.3$; Right: Sketch of the phase portrait for (43) with $\varepsilon \ll 1$, the black circle represents the stationary point.

13. Klumpp, S., Chai, Y., and Lipowsky, R., 2008. *Effects of the chemomechanical stepping cycle on the traffic of molecular motors*. Physical Review E, **78**, 041909.
14. Klumpp, S., Nieuwenhuizen, T. M., and Lipowsky, R., 2005. *Self-organized density patterns of molecular motors in arrays of cytoskeletal filaments*. Biophysical Journal, **88**, pg. 3118-3132.
15. Klumpp, S., and Lipowsky, R., 2005. *Cooperative cargo transport by several molecular motors*. PNAS, **102**(48), pg. 17284-17289.
16. Varga, V., Leduc, C., Bormuth, V., Diez, S., and Howard, J., 2009. *Kinesin-8 motors act cooperatively to mediate length-dependent microtubule depolymerization*. Cell, **138**, pg. 1174-1183.
17. Liang, W. H., Li, Q., Rifat Faysal, K. M., King, S. J., Gopinathan, A., and Xu, J., 2016. *Microtubule defects influence kinesin-based transport in vitro*. Biophysical Journal, **110**, pg. 2229-2240.
18. Mallik, R., and Gross, S. P., 2004. *Molecular motors: Strategies to get along*. Current Biology, **14**, pg. R971-R982.
19. Müller, M. J. I., Klumpp, S., and Lipowsky, R., 2005. *Molecular motor traffic in a half-open tube*. Journal of Physics: Condensed Matter, **17**, pg. S3839-S3850.
20. Rossi, L. W., Radtke, P. K., and Goldman, C., 2014. *Long-range cargo transport on crowded microtubules: The motor jamming mechanism*. Physica A, **401**, pg. 319-329.
21. Striebel, M., Graf, I. R., and Frey, E., 2020. *A mechanistic view of collective filament motion in active nematic networks*. Biophysical Journal, **118**(2), pg. 313-324.
22. Dallon, J. C., Leduc, C., Etienne-Manneville, S., Portet, S., 2019. *Stochastic modeling reveals how motor protein and filament properties affect intermediate filament transport*. Journal of Theoretical Biology, **464**, pg. 132-148.

A Homogeneous microtubules: Proof of Theorem 1 and Corollary 1

Equation (14) may be rewritten in the form of a system of two first order ODEs for density ρ_ε and flux J_ε (see also (11)):

$$\begin{cases} \frac{\varepsilon}{2} \rho'_\varepsilon = -v_0^{-1} J_\varepsilon + \rho_\varepsilon(1 - \rho_\varepsilon), \\ J'_\varepsilon = \Omega_A - (\Omega_A + \Omega_D) \rho_\varepsilon. \end{cases} \quad (43)$$

Next, we discuss the phase portrait for this system with $\varepsilon \ll 1$, depicted in Fig. 4. Away from curve γ defined by

$$\gamma := \left\{ (\rho, J) \mid J = v_0 \rho(1 - \rho) \text{ and } \begin{matrix} 0 \leq \rho \leq 1, \\ 0 \leq J \leq v_0/4 \end{matrix} \right\}, \quad (44)$$

the trajectories of (43), parametrized by $0 \leq x \leq \ell$, have almost horizontal slope in (ρ, J) plane. This is because the slope of ρ_ε is of the order ε^{-1} , that is $\rho'_\varepsilon(x) \sim \varepsilon^{-1}$, whenever the point $(\rho_\varepsilon(x), J_\varepsilon(x))$ is away from γ (it follows from the first equation in (43)). It would be natural to expect that as ε vanishes, trajectory $\{(\rho_\varepsilon(x), J_\varepsilon(x)), 0 \leq x \leq \ell\}$ approaches the arch γ and this trajectory is contained in a given thin neighborhood of γ for sufficiently small ε . In this subsection, it will be shown that the behavior of the solution is more complicated than simply evolving near γ .

To describe how the solution $\rho_\varepsilon(x)$ behaves for $\varepsilon \ll 1$, we introduce the following notation for parts of curve γ . Namely,

$$\begin{aligned}\gamma_l &:= \gamma \cap \{0 \leq \rho < 0.5\}, \\ \gamma_{r,+} &:= \gamma \cap \{0.5 \leq \rho \leq \rho_{\text{eq}}\}, \\ \gamma_{r,-} &:= \gamma \cap \{\rho_{\text{eq}} \leq \rho \leq 1\}.\end{aligned}$$

Here $\rho_{\text{eq}} := \Omega_A/(\Omega_A + \Omega_D)$. Let us also introduce the following horizontal segment

$$\Gamma := \{(\rho, J) : J = v_0/4, 0 \leq \rho \leq 0.5\},$$

and the solution $g(x; s, a)$ to (16), i.e., the initial value problem of the first order obtained by the formal limit as $\varepsilon \rightarrow 0$ in (14):

$$v_0(1 - 2g)\partial_x g = \Omega_A - (\Omega_A + \Omega_D)g, \quad g(s; s, a) = a. \quad (45)$$

First, note that γ_l , which is the left part of the curve γ , is unstable, that is all trajectories, excluding γ_l , are directed away from γ_l in the vicinity of γ_l . The right part of the curve γ , consisting of curve segments $\gamma_{r,+}$ and $\gamma_{r,-}$, is stable, attracting all trajectories in its vicinity, except those that follow Γ . We note that this exception, when $\gamma_{r,+}$ loses its stability, occurs at the interface point $(\rho = 1/2, J = v_0/4)$ where $\gamma_{r,+}$ meets γ_l . All trajectories reaching this point near (not necessarily intersecting) the curves $\gamma_{r,+}$ and γ_l continue along Γ .

Given specific values of $\alpha, \beta \in (0, 1)$ in boundary conditions (15), the statement of Theorem 1 as well as representation formula (20) can be simply verified by careful inspection of the phase portrait depicted in Fig. 4. Specifically, for all $0 < \alpha, \beta < 1$, one can draw a path $\{(\rho(x), J(x)) : 0 \leq x \leq \ell\}$ along arrows in Fig. 4 (right), which starts at vertical line $\rho = \alpha$ and ends at vertical line $\rho = 1 - \beta$, and such a path will be unique for given α and β (see also left column of Fig. 5 for specific examples). Instead of checking each couple (α, β) , one would split ranges of (α, β) into sub-domains within which the outer solution has constant or smoothly varying shape, as it is done in proof below.

Proof of Theorem 1. Consider the following functions:

$$\rho_\alpha(x) = g(x; 0, \alpha) \text{ and } \rho_\beta(x) = g(x; \ell, \max\{0.5, 1 - \beta\}).$$

These functions can be thought of as one-sided solutions (i.e., satisfying one of the boundary conditions, either $\rho(0) = \alpha$ or $\rho(\ell) = \max\{0.5, 1 - \beta\}$) of Equation (14) for $\varepsilon = 0$. The reason we choose $\rho(\ell) = \max\{0.5, 1 - \beta\}$ instead of $\rho_\beta(\ell) = 1 - \beta$ is because there is no solution continuous at $x = \ell$ with $\rho(\ell) < 0.5$ as visible in Fig. 4 (curve γ is unstable in region $\{0 \leq \rho < 0.5\}$).

Introduce also the corresponding fluxes:

$$J_\alpha(x) = v_0\rho_\alpha(x)(1 - \rho_\alpha(x)) \text{ and } J_\beta(x) = v_0\rho_\beta(x)(1 - \rho_\beta(x)).$$

From the definition of function g it follows that $J_\alpha(x)$ and $J_\beta(x)$ are both monotonic functions, and function $J_\beta(x)$ is defined for all $0 \leq x < \ell$. Moreover, $J_\beta(x)$ can be extended onto $(-\infty, \ell]$ and

$$\lim_{x \rightarrow -\infty} J_\beta(x) = J_{\text{eq}}, \text{ where } J_{\text{eq}} := v_0 \frac{\Omega_A \Omega_D}{(\Omega_A + \Omega_D)^2}.$$

Consider case $\alpha \geq 0.5$. From Fig. 4, it follows that a trajectory emanating for initial point (α, J) for any $0 < J < v_0/4$ immediately reaches γ_r and stays on $\gamma_r \cup \Gamma$ for $0 < x \leq \ell$. Thus, at $x = 0$ trajectory $\{(\rho_0(x), J_0(x)) : 0 \leq x \leq \ell\}$, describing the outer solution, jumps from $(\alpha, J_0(0))$ at $t = 0$ to γ_r :

$$\rho_0(x) = \begin{cases} \alpha, & x = 0, \\ \rho_\beta(x), & 0 < x \leq \ell. \end{cases} \quad (46)$$

In the case where $\alpha < 0.5$, denote by $0 \leq x_J \leq \ell$ location at which fluxes $J_\alpha(x)$ and $J_\beta(x)$ intersect, that is,

$$J_\alpha(x_J) = J_\beta(x_J). \quad (47)$$

Equality (47) implies that either $\rho_\alpha(x_J) = 1 - \rho_\beta(x_J)$ or $\rho_\alpha(x_J) = \rho_\beta(x_J)$. If $\rho_\alpha(x_J) = \rho_\beta(x_J)$, then since ρ_α and ρ_β are solutions of the same first order ordinary differential equation, these two functions coincide $\rho_\alpha(x) \equiv \rho_\beta(x)$.

We show now that either

$$\text{there exists at most one } x_J \leq 1 \text{ or } \rho_\alpha(x) \equiv \rho_\beta(x). \quad (48)$$

Indeed, since $\alpha < 0.5$, trajectory $(\rho_\alpha(x), J_\alpha(x))$ evolves on γ_l for all $0 \leq x \leq \ell$ where solution $\rho_\alpha(x)$ exists, and $J_\alpha(x)$ monotonically increases. Trajectory $(\rho_\beta(x), J_\beta(x))$ evolves also for all $0 \leq x \leq \ell$ within either $\gamma_{r,+}$ or $\gamma_{r,-}$. If $(\rho_\beta(x), J_\beta(x))$ evolves within $\gamma_{r,-}$, then $J_\beta(x)$ is monotonically decreasing in x whereas $J_\alpha(x)$ is monotonically increasing x , and thus equation $J_\alpha(x) = J_\beta(x)$ can have at most one root in this case. If $(\rho_\beta(x), J_\beta(x))$ evolves within $\gamma_{r,+}$, then both $J_\alpha(x)$ and $J_\beta(x)$ increase with x . Assume that there are at least two distinct numbers $x_J^{(1)}, x_J^{(2)}$ such that $x_J^{(1)} < x_J^{(2)}$ and $J_\alpha(x_J^{(i)}) = J_\beta(x_J^{(i)})$, $i = 1, 2$. Assume also that $x_J^{(1)}$ and $x_J^{(2)}$ are neighbor roots of equation $J_\alpha(x) = J_\beta(x)$, i.e., for all $x \in (x_J^{(1)}, x_J^{(2)})$ we have $J_\alpha(x) \neq J_\beta(x)$. Then due to

$$\partial_x J = \Omega_A - (\Omega_A + \Omega_D)g, \text{ where } J(x) = v_0 g(x)(1 - g(x))$$

and $\rho_\alpha(x_J^{(i)}) < 0.5$ $\rho_\alpha(x_J^{(i)}) > 0.5$, $i = 1, 2$, we have that $\partial_x J_\alpha(x_J^{(i)}) > \partial_x J_\beta(x_J^{(i)})$, $i = 1, 2$. Noting that a smooth function can't have the same sign of its derivative at two successive roots we arrive to contradiction. Therefore, such x_J is at most one and (48) is shown.

If $J_\alpha(x) \neq J_\beta(x)$ for all $0 \leq x \leq 1$, then define x_J as follows:

$$x_J = \begin{cases} 0, & J_\beta(x) < J_\alpha(x) \text{ for all } 0 < x < \ell, \\ 1, & J_\alpha(x) < J_\beta(x) \text{ for all } 0 < x < \ell. \end{cases}$$

We note that point $x = x_J$ is where the outer solution jumps from $\rho_\alpha(x)$ to $\rho_\beta(x)$, thus

$$\rho_0(x) = \begin{cases} \rho_\alpha(x), & 0 \leq x < x_J, \\ \rho_\beta(x), & x_J < x < \ell. \end{cases} \quad (49)$$

and $\rho_0(\ell) = 1 - \beta$.

Formulas (46), (49), and (15) complete the proof of Theorem 1. \square

B Examples of solutions given by (20)

To illustrate the result of Theorem 1 we continue with the following examples. We take $v_0 = 1$, $\ell = 1$, $\Omega_A = 0.8$ and $\Omega_D = 0.2$, and we vary the boundary rates α and β . The outer solution for each example, as both a trajectory in (ρ, J) plane and the plot of $\rho_0(x)$, is depicted in Fig. 5.

Example 1. $\alpha = 0.4$ and $\beta = 0.39$.

$$\rho_0(x) = \begin{cases} 0.4, & x = 0 \\ g(x; 1, 0.61), & 0 < x \leq 1. \end{cases}$$

Example 2. $\alpha = 0.1$ and $\beta = 0.4$.

$$\rho_0(x) = \begin{cases} g(x; 0, 0.1), & 0 \leq x \leq x_J, x_J \approx 0.133 \\ g(x; 1, 0.6), & x_J < x \leq 1. \end{cases}$$

Example 3. $\alpha = 0.1$ and $\beta = 0.85$.

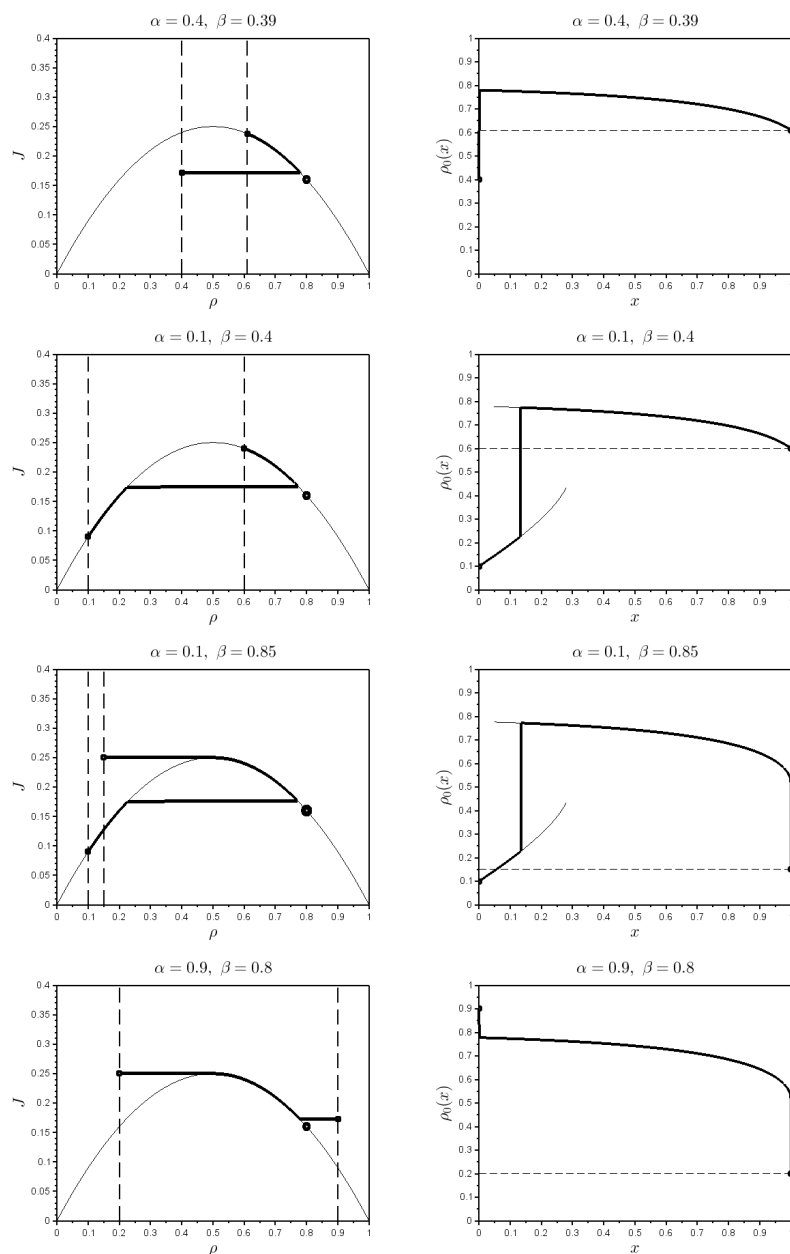


Fig. 5 Left: The thick line represents the trajectories from Examples 1-4; it starts at $\rho = \alpha$ and ends at $\rho = 1 - \beta$, the black circle at $(0.8, 0.16)$ represents the stationary solution. Right: The thick line represents the outer solution $\rho_0(x)$ for Examples 1-4. In Examples 2 and 3, branches $g(x; 0, \alpha)$ and $g(x; 1, \max\{0.5, 1 - \beta\})$ extend slightly beyond the intervals where they are a part of the outer solution $\rho_0(x)$ (thin curves).

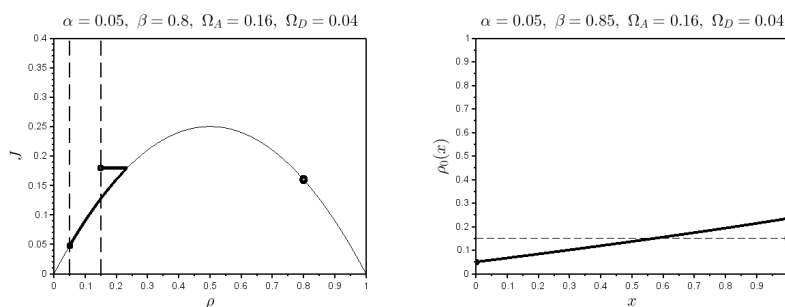


Fig. 6 The thick line represents the trajectories from Example 5; it starts at $\rho = \alpha$ and ends at $\rho = 1 - \beta$, the black circle at $(0.8, 0.16)$ represents the stationary solution. Right: The thick line represents the outer solution $\rho_0(x)$ for Example 5.

$$\rho_0(x) = \begin{cases} g(x; 0, 0.1), & 0 \leq x \leq x_J, x_J \approx 0.135, \\ g(x; 1, 1/2), & x_J < x < 1, \\ 0.15, & x = 1. \end{cases}$$

Example 4. $\alpha = 0.9$ and $\beta = 0.8$.

$$\rho_0(x) = \begin{cases} 0.9, & x = 0, \\ g(x; 1, 1/2), & 0 < x < 1, \\ 0.2, & x = 1. \end{cases}$$

The case $x_J > 1$ corresponds to the case of fast motor proteins or, more precisely, unidirectional motion dominates attachment/detachment, and thus resulting density is low in MT, $\rho_0(x) < 0.5$ for $x \in (0, 1)$. Consider the following example:

Example 5. $\alpha = 0.05$, $\beta = 0.85$, $\Omega_A = 0.16$ and $\Omega_D = 0.04$.

$$\rho_0(x) = \begin{cases} g(x, 0, \alpha), & 0 \leq x < 1, \\ 1 - \beta, & x = 1. \end{cases}$$

The solution is depicted in Fig. 6.